# Residue F4 Plays a Key Role in Modulating Oxygen Affinity and Cooperativity in *Scapharca* Dimeric Hemoglobin†

James E. Knapp, Michele A. Bonham, Quentin H. Gibson, Jeffry C. Nichols, and William E. Royer, Jr.*

*Department of Biochemistry and Molecular Pharmacology, University of Massachusetts Medical School, Worcester, Massachusetts 01655*

*Received June 2, 2005; Revised Manuscript Received September 2, 2005*

ABSTRACT: Residue F4 (Phe 97) undergoes the most dramatic ligand-linked transition in *Scapharca* dimeric hemoglobin, with its packing in the heme pocket in the unliganded (T) state suggested to be a primary determinant of its low affinity. Mutation of Phe 97 to Leu (previously reported), Val, and Tyr increases oxygen affinity from 8- to 100-fold over that of the wild type. The crystal structures of F97L and F97V show side chain packing in the heme pocket for both R and T state structures. In contrast, in the highest-affinity mutation, F97Y, the tyrosine side chain remains in the interface (high-affinity conformation) even in the unliganded state. Comparison of these mutations reveals a correlation between side chain packing in the heme pocket and oxygen affinity, indicating that greater mass in the heme pocket lowers oxygen affinity due to impaired movement of the heme iron into the heme plane. The results indicate that a key hydrogen bond, previously hypothesized to have a central role in regulation of oxygen affinity, plays at most only a small role in dictating ligand affinity. Equivalent mutations in sperm whale myoglobin alter ligand affinity by only 5-fold. The dramatically different responses to mutations at the F4 position result from subtle, but functionally critical, stereochemical differences. In myoglobin, an eclipsed orientation of the proximal His relative to the A and C pyrrole nitrogen atoms provides a significant barrier for high-affinity ligand binding. In contrast, the staggered orientation of the proximal histidine found in liganded HbI renders its ligand affinity much more susceptible to packing contacts between F4 and the heme group. These results highlight very different strategies used by cooperative hemoglobins in molluscs and mammals to control ligand affinity by modulation of the stereochemistry on the proximal side of the heme.

The dimeric hemoglobin (HbI)[1] from the blood clam *Scapharca inaequivalvis* is an ideal model system in which to study allosteric behavior because of the presence of two chemically identical binding sites and relatively localized ligand-linked structural transitions. HbI binds oxygen cooperatively, with a Hill coefficient of 1.5 for equilibrium oxygen binding and with no modulation of oxygen affinity by non-heme binding ligands such as bisphosphoglycerate (BPG), protons, carbon dioxide, or chloride ions (*1*). High-resolution crystallographic analysis shows that this dimer is formed primarily through contacts between the E and F helices of each subunit (*2*), which is entirely different from the assemblage observed in the well-known vertebrate tetrameric hemoglobin (*3*). Nevertheless, EF dimer assemblages are widespread among cooperative invertebrate hemoglobins, having been observed crystallographically in the dimeric Hb D from the echinoderm sea cucumber *Caudina arenicola* (*4*) and as substructures of the heterotetrameric HbII from the mollusc *S. inaequivalvis* (*5*), the giant respiratory complex from the annelid *Lumbricus terrestris* (*6*), and the 400 kDa hemoglobin from the hydrothermal vent tubeworm *Riftia pachyptila* (*7*).

The EF assemblage brings the two heme groups within the dimer close together, allowing tertiary rather than quaternary structural transitions to mediate cooperativity. Site-directed mutagenesis has confirmed the functional importance of three major ligand-linked structural changes observed from comparison between the liganded and unliganded crystal structures. These include the ligand-linked movement of the heme groups (*8*), the conformational change of Phe 97 (F4) (*9*), and the change in the arrangement of a water cluster located at the dimer interface (*10*). Despite striking changes at the subunit interface, quaternary transitions are limited to a 3.3° subunit rotation. This quaternary change is, however, an integral component of the HbI transitions, as evidenced in situ when the CO ligand is removed from HbI−CO crystals (*11*).

Phe 97 undergoes the largest structural rearrangement once a ligand binds to HbI. In the absence of ligand, Phe 97 (F4) packs in the heme pocket against the proximal histidine F8 (His 101), which restricts the heme iron from moving into the heme plane and lengthens a crucial hydrogen bond between the proximal histidine and the main chain carbonyl oxygen of Phe F4 (*2*). (By convention, individual residues are designated by the homologous helical position in sperm whale myoglobin, the first globin structure determined. Thus, the proximal histidine is designated as F8, the eighth residue

† This work was supported by the National Institutes of Health (Grant DK43323 to W.E.R.).

* To whom correspondence should be addressed. Phone: (508) 845-6912. Fax: (508) 856-6464. E-mail: william.royer@umassmed.edu.

[1] Abbreviations: Hb, hemoglobin; HbI, *Scapharca* dimeric hemoglobin I; Mb, myoglobin; $p_{50}$, partial pressure of oxygen at which 50% of ligand binding sites are occupied; rms, root-mean-square.

10.1021/bi051052+ CCC: $30.25 
Published on Web 10/07/2005

of the F helix in myoglobin, even though it is the 15th residue in the F helix of HbI.) Both of these effects have been proposed to lower oxygen affinity in the low-affinity T state, observed in the unliganded structure. Once a ligand binds, the Phe 97 side chain moves from the proximal heme pocket into the subunit interface, where it disrupts a cluster of well-ordered water molecules. This transition to the high-affinity R state relieves the strain in the proximal pocket, permitting the iron to freely move into the heme plane and a strong hydrogen bond to be formed between the proximal His and main chain carbonyl oxygen of Phe 97 (*2*). Substituting a leucine at position 97 confirms the central role of this residue, leading to an 8-fold increase in oxygen affinity and a greatly reduced, but not eliminated, level of cooperative ligand binding (*9*). Kinetic analysis suggests elimination of the proximal contributions to cooperativity in the F97L mutation.

We report here the results of two additional substitutions at position F4, to Val and Tyr. These mutations have a much greater functional impact than does the Leu mutation, and these mutants also exhibit more dramatic functional changes than homologous mutants of sperm whale myoglobin. These results highlight a cooperative ligand binding strategy in HbI in which the orientation of the proximal histidine permits strong modulation of oxygen affinity by altering the packing of the F4 residue.

## EXPERIMENTAL PROCEDURES

*Mutagenesis, Expression, and Purification*. The F97Y mutation was introduced into the HbI plasmid pCS26 using cassette mutagenesis as described by Pardanani et al. (*9*). The F97V mutation was made with the PCR protocol of Statagene (QuickChange) as described previously (*8*). All mutations were expressed in *Escherichia coli* W3110lacIq L8, and purified using the procedure for recombinant wild-type HbI (*12*).

*Functional Analysis of the Mutations.* Equilibrium oxygen binding measurements were carried out using using tonometric methods at 23 °C in solutions with a Hb concentration of 50 $\mu$M heme at pH 7.2 as described previously (*10*). Absorbance values for each step of oxygen addition were monitored at nine different wavelengths in the visible range. The measured absorbance differences were used for a Hill plot analysis, from which the $p_{50}$ (partial pressure at which 50% of $O_2$ binding sites are occupied) and Hill coefficient ($n$) were determined. A reducing enzyme system was used to maintain the redox state of HbI (*13*). This reducing system was especially important for F97V, because of its susceptibility to oxidation, but not for F97Y, F97V, and the wild type, which are quite resistant to oxidation. There was no clear correlation between oxygen affinity and susceptibility to oxidation, as the F97L and F97Y mutants have lower and higher affinities, respectively, than F97V but both show strong resistance to oxidation.

Measurements of CO and $O_2$ reaction rates were monitored following flash photolysis initiated either with a 4−6 ns pulse at 532 nm from a Q-switched YAG laser (Continuum Surelite SLI-10) similar to that described by Scott and Gibson (*14*) or with a Sunpak auto544 thyristor. The flash from the Sunpak was concentrated on the sample using a plexiglass light guide, 90° from the observation beam. A yellow filter was used to block light from the flash of wavelengths below approximately 460 nm right after the flash head. The observation beam is from a 150 W halogen bulb, with blue filters used on either side of the sample, limiting observing light to the 300−500 nm range. The signal from a Bauch and Lomb monochrometer was collected via a photomultiplier tube and sent to a Tektronix TDS 620 oscilloscope. The raw data were collected using IGOR Pro version 4 for further analysis. Observation was continued throughout the flash, and the resulting traces were modeled using the flash profile as a forcing function.

Table 1: Kinetic Ligand Binding Properties of F97 Mutants[a]

| | oxygen on rates | | oxygen off rates | | CO on rates | |
|---|---|---|---|---|---|---|
| | $k_1'$ ($\mu M^{-1}$ $s^{-1}$) | $k_2'$ ($\mu M^{-1}$ $s^{-1}$) | $k_1$ ($s^{-1}$) | $k_2$ ($s^{-1}$) | $l_1'$ ($\mu M^{-1}$ $s^{-1}$) | $l_2'$ ($\mu M^{-1}$ $s^{-1}$) |
| HbI | 10 | 16 | 500 | 73 | 0.09 | 0.2 |
| F97L | 18 | 23 | 100 | 31 | 0.9 | 1.8 |
| F97V | 27 | 47 | 13 | 4.1 | 4.2 | 4.2 |
| F97Y | 47 | 47 | 2.3 | 2.3 | 4.3 | 4.3 |

[a] Subscripts define the binding step based on a consecutive two-step scheme following Adair (*31*) using the procedure described in Experimental Procedures. A prime designates an on rate, and the lack of a prime designates an off rate.

Kinetic experiments on oxygenated mutants were performed using laser photolysis. The low quantum yield for photodissociation of oxygen together with extensive geminate recombination restricts the extent of photolysis. There was no systematic change in the rate constant either with the level of photolysis or with the concentration of oxygen. The observed rate is therefore taken as a measure of $k_2'$ (Table 1).

Binding of CO alone was followed at a series of levels of photodissociation using Sunpak and laser photolysis. Data were measured at various levels of photolysis. Close to full photolysis, the initial rate gives an estimate of the rate of binding of the first CO molecule ($l_1'$), while a low level of photolysis approximates the rate of binding of the second CO molecule ($l_2'$). To obtain estimates of other rates, solutions were equilibrated with gas mixtures containing relatively small amounts of $O_2$ (<6%) with the balance either 10% CO and $N_2$ or 100% CO. Flash photolysis of the solutions removes CO rapidly. The unliganded $Hb_2$ form combines mainly with $O_2$, with an observed rate that reflects the sum of the combination and dissociation rates. Subsequently, and on a much longer time scale, oxygen is replaced with CO, completing the cycle.

To extract the rates of the oxygen reactions, all of the data described, together with equilibrium data, are represented by the kinetic equivalent of the MWC model (*15*) using a model as previously described (*8*). The rate at each step is the rate for the T state multiplied by the proportion of T state plus the R state rate multiplied by its proportion. The results are given in Table 1. In effect, the model is used as a smoothing function for the data.

*Crystallographic Analysis.* Crystals of both states for F97V and F97Y were grown in batch experiments under conditions used to crystallize the corresponding form of wild-type HbI (*2*). CO-liganded crystals were grown under an atmosphere of carbon monoxide in solutions that were 2.1−2.4 M phosphate buffer at pH 7.5, whereas the unliganded crystals were grown in an anaerobic chamber (Anaerobe Systems, Morgan Hill, CA) in solutions that were 1.9−2.2 M phosphate buffer at pH 8.5. The CO-liganded crystals show

Table 2: Data Collection and Refinement Statistics

| | F97V−CO | d-F97V | F97Y−CO | d-F97Y |
|---|---|---|---|---|
| space group | *C*2 | $C222_1$ | *C*2 | $C222_1$ |
| cell constants | | | | |
| *a* (Å) | 93.1 | 92.0 | 93.3 | 92.1 |
| *b* (Å) | 43.9 | 44.4 | 44.0 | 44.3 |
| *c* (Å) | 83.5 | 143.8 | 83.6 | 143.9 |
| $\beta$ (deg) | 121.9 | 90.0 | 122.0 | 90.0 |
| completeness | 85.3 (68.6) | 88.2 (78.0) | 97.8 (98.8) | 87.4 (78.2) |
| multiplicity | 2.5 | 2.3 | 3.3 | 3.2 |
| $I/\sigma(I)$ | 12.6 (4.9) | 8.8 (3.9) | 23.2 (4.2) | 17.0 (3.9) |
| $R_{sym}$ overall (highest-resolution shell) | 0.063 (0.158) | 0.098 (0.253) | 0.064 (0.326) | 0.053 (0.321) |
| resolution range (Å) | 40−1.8 | 40−2.3 | 40−1.5 | 40−1.8 |
| total no. of reflections ($F > 1\sigma$) | 26828 | 11945 | 40980 | 24393 |
| no. of reflections in the $R_{free}$ test set | 2262 | 959 | 4056 | 4566 |
| *R*-factor | 0.180 | 0.190 | 0.193 | 0.178 |
| $R_{free}$ | 0.214 | 0.241 | 0.213 | 0.205 |
| no. of non-hydrogen atoms | | | | |
| protein | 2224 | 2224 | 2234 | 2234 |
| heme and ligand | 90 | 86 | 90 | 86 |
| solvent | 164 | 80 | 190 | 188 |
| no. of alternate conformations | 4 | 0 | 2 | 1 |
| average *B*-factor (Å$^2$) | | | | |
| main chain atoms | 17.7 | 20.6 | 15.6 | 20.9 |
| side chain atoms | 23.1 | 25.9 | 18.6 | 25.0 |
| heme atoms | 17.8 | 18.8 | 13.4 | 22.6 |
| CO ligands | 16.0 | − | 13.1 | − |
| solvent atoms | 34.8 | 34.1 | 28.5 | 40.3 |
| core interface waters | 27.5 | 27.3 | 24.7 | 40.4 |
| rms deviation from ideal value | | | | |
| bond lengths (Å) | 0.005 | 0.005 | 0.006 | 0.006 |
| bond angles (deg) | 0.93 | 1.22 | 1.12 | 1.34 |
| dihedral angles (deg) | 17.8 | 17.6 | 19.0 | 17.8 |
| improper angles (deg) | 0.84 | 1.00 | 0.99 | 0.92 |
| Ramachandran plot (%) | | | | |
| most favored regions | 95.0 | 93.5 | 95.8 | 96.2 |
| allowed regions | 5.0 | 6.5 | 4.2 | 3.8 |

the symmetry of space group *C*2, with an intact dimer per asymmetric unit. Crystals of unliganded F97V and F97Y show the symmetry of space group $C222_1$, also having an intact dimer per asymmetric unit (Table 2). X-ray diffraction data were collected on an R-axis IIC image plate system as described previously (*8*). The measured intensities for each data set were processed, scaled, and merged with the HKL package (*16*) before being converted to structure factors with the CCP4 program Truncate (*17*). A subset (between 5 and 10%) of the data was set aside for the calculation of $R_{free}$ (*18*) for crystallographic refinement.

The *C*2 and $C222_1$ crystal forms of the two mutants are isomorphous to crystals of CO-liganded HbI (PDB entry 4SDH) and unliganded HbI (PDB entry 3SDH). Phases were calculated from HbI models that were correctly placed in each unit cell by rigid-body refinement. The initial model included the main chain and side chain atoms, but with position 97 truncated to an alanine. The models of F97Y−CO and unliganded F97Y−CO complexes were initially optimized with two rounds of simulated annealing and individual *B*-factor refinement with XPLOR (*19*). Water molecules were added after each round of refinement with XPLOR based on $2F_o - F_c$ and $F_o - F_c$ electron density maps along with the presence of suitable hydrogen bonding partners. Alternate conformations were added, and the model underwent positional and individual *B*-factor refinement with CNS (*20*). The unliganded and CO forms of F97V were refined with multiple rounds of computational refinement with CNS and manual intervention with O (*21*). Each round of refinement included positional refinement and either the optimization of individual *B*-factors (CO−F97V) or the optimization of a main chain and side chain *B*-factor (unliganded F97V). Water molecules were placed into the model with CNS and were removed if electron density was not present in omit $2F_o - F_c$, $\sigma$A weighted omit maps or if no hydrogen bond partners were available. Alternate side chain conformations were added to the CO−F97V form during the last round of refinement.

The refined models of the liganded and unliganded forms of both F97V and F97Y mutants include residues 2−146, with the N-terminal Pro being disordered. The F97V−CO model includes four residues with alternate side chain conformations (Lys 16, Ile 71, and Val 90 from the A subunit and Lys 15 from the B subunit). The F97Y−CO model includes two residues (Met 37 from the A subunit and Val 93 from the B subunit) with alternate side chain conformations. The unliganded F97Y model has one side chain with alternate conformations (Lys 96 from the B subunit), whereas the unliganded F97V model does not include any alternate side chain conformations. All models show good agreement with the observed data as indicated by $R_{free}$ values between 20.5 and 24.1% and show excellent agreement with ideal model geometry (Table 2). The coordinates and diffraction data describing the CO-ligated and unliganded forms of F97V (PDB entries 2AUQ and 2AUR) and F97Y (PDB entries 2AUO and 2AUP) have been deposited in the Protein Data Bank (PDB) (*22*).

The models of liganded and unliganded F97L underwent an additional round of energy minimization with CNS to improve the heme geometry to facilitate the comparison of

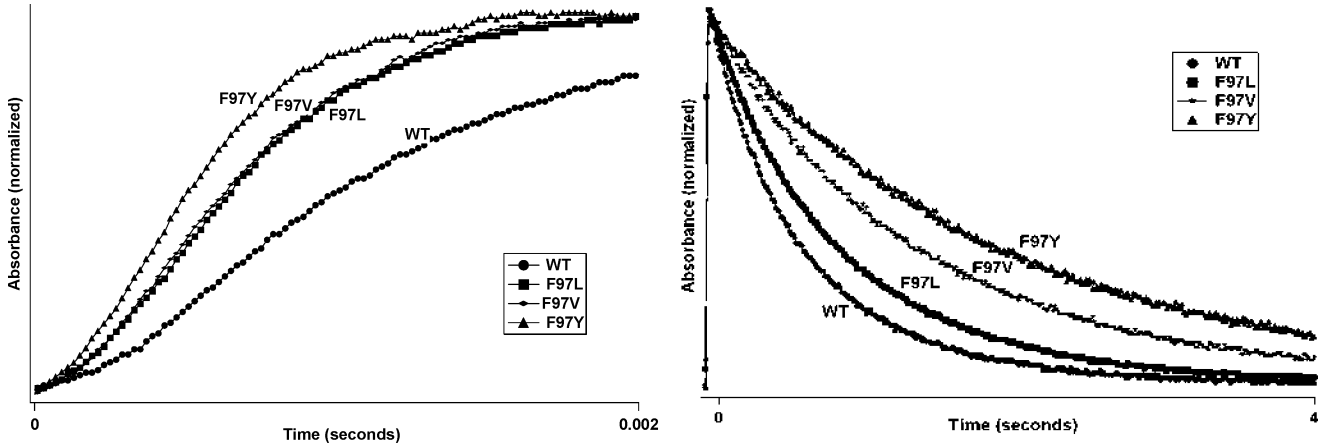


FIGURE 1: $O_2$/CO replacement kinetics on wild-type HbI, F97L, F97V, and F97Y. Each curve shows the raw data from samples equilibrated with 10% CO along with 71 $\mu$M $O_2$. The full reaction following a Sunpak flash is monitored for 4 s (right) with the initial 2 ms of the reaction shown at the left. The initial phase of the reaction represents primarily the rapid binding of oxygen following photolysis of CO. The sigmoidal shape of these curves results from the effects of the Sunpak flash, which extends ~1 ms into the traces that are shown. (The kinetic parameters provided in Table 1 have been corrected for the measured lamp profile.) During the longer phase of the reaction at the right, oxygen is replaced with CO. Note the very rapid binding of oxygen by F97Y (left) and its slow release (right).

this mutation with the other two F4 mutations. The newly refined structures of CO-liganded and unliganded F97L have been deposited in the PDB as entries 2AVO and 2AV3, respectively.

Least-squares superposition calculations were conducted with LSQMAN (*23*), and the least-squares definition of heme planes was carried out with programs of the CCP4 package (*17*). The coordinates of wild-type sperm whale myoglobin (PDB entry 1A6N) (*24*), L89F (PDB entry 1CH2), and L89G (PDB entry 1CH1) (*25*) that were used to make Figure 7 were superimposed upon their unliganded HbI counterparts with LSQMAN (*23*).

## RESULTS

*Functional Properties of Phe F4 Mutants.* Equilibrium oxygen binding experiments confirm the profound effect of altering the residue at position F4 in HbI. Mutation of Phe 97 to Leu raises oxygen affinity by ~8-fold to 1 Torr, as previously reported (*9*). Substitution of a Val at this position increases the oxygen affinity to 0.3 Torr, whereas replacement with a Tyr increases the oxygen affinity to 0.08 Torr, the highest known affinity for any mutant of HbI. The substantial increase in oxygen affinity is coupled with a severe attenuation of cooperative oxygen binding, as indicated by the Hill coefficients, which vary between 1.1 and 1.2 for these mutants.

Kinetic experiments on the F97 mutants provide a more detailed understanding of the ligand binding properties. Flash photolysis experiments, including oxygen/CO replacement reactions (Figure 1), as described in Experimental Procedures have been carried out on all three mutants as well as wild-type HbI. Table 1 provides kinetic rate constants. From these experiments, the following picture emerges. Combination rate constants for oxygen and CO follow the pattern of the wild type being slowest, followed by F97L and F97V with ligands binding most rapidly to F97Y. The oxygen dissociation constants are fastest with the wild type, followed by F97L then F97V with the slowest dissociation rate for F97Y. Thus, the kinetic parameters for these mutants are entirely consistent with the equilibrium oxygen affinity measurements showing the following order of oxygen affinity: F97Y > F97V > F97L > wild type. As is evident in Figure 1, the very high affinity of F97Y is reflected in rapid oxygen combination and slow oxygen release. Evidence of cooperativity, as changes in the binding rates for the first and second step of ligation, is apparent for F97L and F97V (Table 1), but not F97Y. It is interesting that F97V and F97L show very similar oxygen combination rates, but rather different oxygen release rates, suggesting that access of ligands to the binding site is similar in both mutants, but that oxygen is more stably bound in F97V than in F97L.

*Crystal Structures of F97Y.* Crystals of CO-liganded and unliganded forms of F97Y are isomorphous to those of wild-type HbI. An atomic model for the F97Y−CO form has been refined at 1.5 Å resolution to a conventional *R*-factor of 0.193 ($R_{free}$ = 0.213), while an atomic model for unliganded F97Y has been refined at 1.8 Å resolution to a conventional *R*-factor of 0.178 ($R_{free}$ = 0.205). Model statistics are provided in Table 2. Electron density maps clearly show the mutant Tyr residue, which remains in the dimeric interface in both ligand states (Figure 2).

The introduction of a Tyr at position 97 does not significantly alter the overall structure of either the R or T state when compared to the wild type. The superposition of each subunit (residues 10−146) from the F97Y−CO form and unliganded F97Y onto their counterparts from the HbI−CO form and unliganded HbI gives average rms deviations of 0.07 and 0.18, respectively. Furthermore, the quaternary subunit arrangement in F97Y is similar to that of the wild type, with the two subunits in the unliganded T state form of F97Y differing from that of the wild-type T state by 0.31°, and the relationship between the two F97Y subunits in its R state assemblage differs from that of the wild-type R state by 0.15°. The quaternary response to ligand binding is slightly attenuated with ligand binding to F97Y coupled with a 3.0° rotation of subunits, while ligand binding to wild-type HbI is coupled with a 3.3° rotation of subunits. Despite the overall similarity between the wild type and F97Y, this substitution results in several important structural differences that underlie the dramatically increased oxygen affinity. The presence of a hydroxyl group on Tyr compared to Phe has two potential effects. The larger side chain will prevent

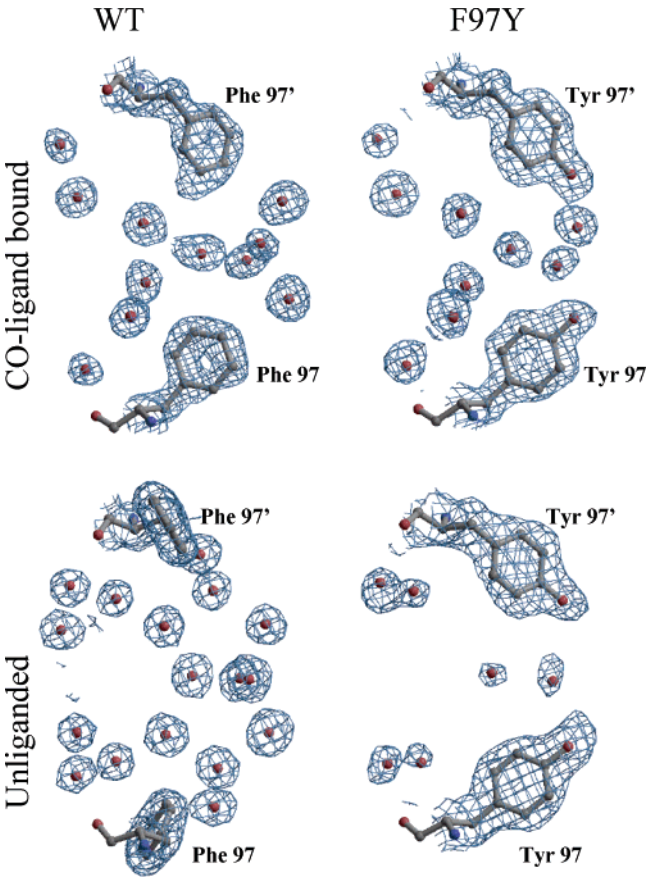


FIGURE 2: Electron density maps for F97Y (right) and wild-type HbI (left), with models of unliganded (top) and CO-liganded (bottom) forms superimposed. For F97Y, simulated annealing, $F_o - F_c$, omit electron density maps are shown at the 3$\sigma$ level in which residue 97 and interface waters were omitted from the phase calculations. For the wild type, $2F_o - F_c$ maps are shown at the 1$\sigma$ level. Maps for wild-type HbI were calculated at 1.8 and 1.5 Å for the unliganded and CO-liganded forms, respectively, to be equivalent to those for F97Y. Tyr 97 adopts essentially the same conformation independent of the presence or absence of ligand, but the water structure changes, with fewer and less well ordered water molecules in the unliganded interface. This is the only HbI mutant to date in which the liganded state is more hydrated than the unliganded state. Figures 2, 5, and 7 were made with BOBSCRIPT (*32*) and RASTER3D (*33*).

packing in the proximal pocket as does Phe 97 in the T state form of wild-type HbI, and additionally, the hydroxyl group may render this side chain more tolerant of being in the hydrated subunit interface. As a result, the phenol ring remains in the dimeric interface in the unliganded structure, similar to the R state position of Phe 97 of wild-type HbI.

*Crystal Structures of F97V.* Crystals of CO-liganded and unliganded forms of F97V are isomorphous to those of wild-type HbI. An atomic model for the F97V−CO form has been refined at 1.8 Å resolution to a conventional *R*-factor of 0.180 ($R_{free}$ = 0.214), while an atomic model for unliganded F97V has been refined at 2.3 Å resolution to a conventional *R*-factor of 0.190 ($R_{free}$ = 0.241) (Table 2).

The overall structure of F97V is very similar to that of the wild type as indicated by rms deviations of 0.09 and 0.17 Å for 137 Cα atoms when subunits of the F97V−CO form and unliganded F97V, respectively, are superimposed upon their counterparts. The F97V substitution also does not greatly alter the relative orientation of either state as the subunit orientations of the R state and T state differ by 0.16° and 0.23°, respectively, relative to that of the wild type. The overall ligand-linked quaternary subunit rotation is 3.3° in both F97V and the wild type. However, the introduction of a Val at F4, like F97Y, substantially alters the proximal pocket and dimeric interfaces of both allosteric states.

The orientation of Val 97 places the $\gamma$1-carbon of Val 97 near the position of the $\gamma$-carbon of Phe 97 where it occupies its T state conformation in the wild type, and places the $\gamma$2-carbon of Val 97 near the position occupied by the $\gamma$-carbon of Phe 97 in its R state conformation in the wild type. Thus, the F97V substitution assumes a conformation that is somewhat intermediate between those of the F97L and F97Y substitutions.

*Packing of Residue F4 in the Proximal Pocket.* Structural differences in the vicinity of residue F4 among wild-type HbI, F97L, F97Y, and F97V are outlined in Figure 3. Ligand affinity is affected by the packing of residue F4 in the heme pocket due to its impact on the reactivity of the heme iron. At least three different stereochemical effects of residue packing in the heme pocket may contribute to modulation of heme iron reactivity: (1) impact on a hydrogen bond involving the proximal histidine, (2) tight packing against the heme, and (3) tight packing against the proximal histidine.

It has been proposed that a strong hydrogen bond between the main chain carbonyl oxygen of residue F4 and proximal histidine can enhance ligand affinity by stabilizing a partial positive charge on the proximal histidine that results from the binding of electron-withdrawing ligands, such as oxygen, to the heme iron (*26*). This hydrogen bond is significantly longer, and thus weaker, in unliganded HbI than in the HbI−CO form (Figure 3) as a result of the packing of Phe 97 in the proximal pocket. In all F4 mutants, this hydrogen bond is reasonably optimal, with bond lengths of 2.8−2.9 Å in both T and R states (Table 3). Thus, this hydrogen bond may contribute to the higher affinity of these mutants compared with that of the wild type, but apparently plays no role in the quite dramatic differences in affinity between mutants.

A second consequence of mutation at residue F4 results from the packing of its side chain against the heme. There is a tight contact in the T state of wild-type HbI between the F4 phenyl ring and the bridging methylene carbon (CHB) between the A and B pyrrole rings, with a contact distance of 3.5 Å (Table 3). This contact is loosened in F97L, with a distance of 3.8 Å, whereas the contact is essentially missing in F97V and F97L, with closest distances of 4.5 and 5.2 Å, respectively (Table 3). The loosening of this contact may increase oxygen affinity by releasing impediments to the movement of the heme iron into the heme plane upon ligand binding.

A third consequence of mutation at residue F4 results from changes in the packing of this residue against the F8 proximal histidine, as Phe 97 also packs tightly against F8 in the T state of wild-type HbI. In the unliganded structure of the wild type, the closest contact between the side chain of residue 97 and the proximal histidine is 3.3 Å, in F97L the closest contact 3.4 Å, in F97V the closest contact 3.9 Å, and in F97Y the closest contact 5 Å. One impact of tight packing between F4 and F8 is alteration of the orientation of the F8 imidazole ring, as shown in Figure 4. The proximal His in the HbI−CO form displays a relatively "staggered" orientation relative to the heme nitrogen atoms from the A

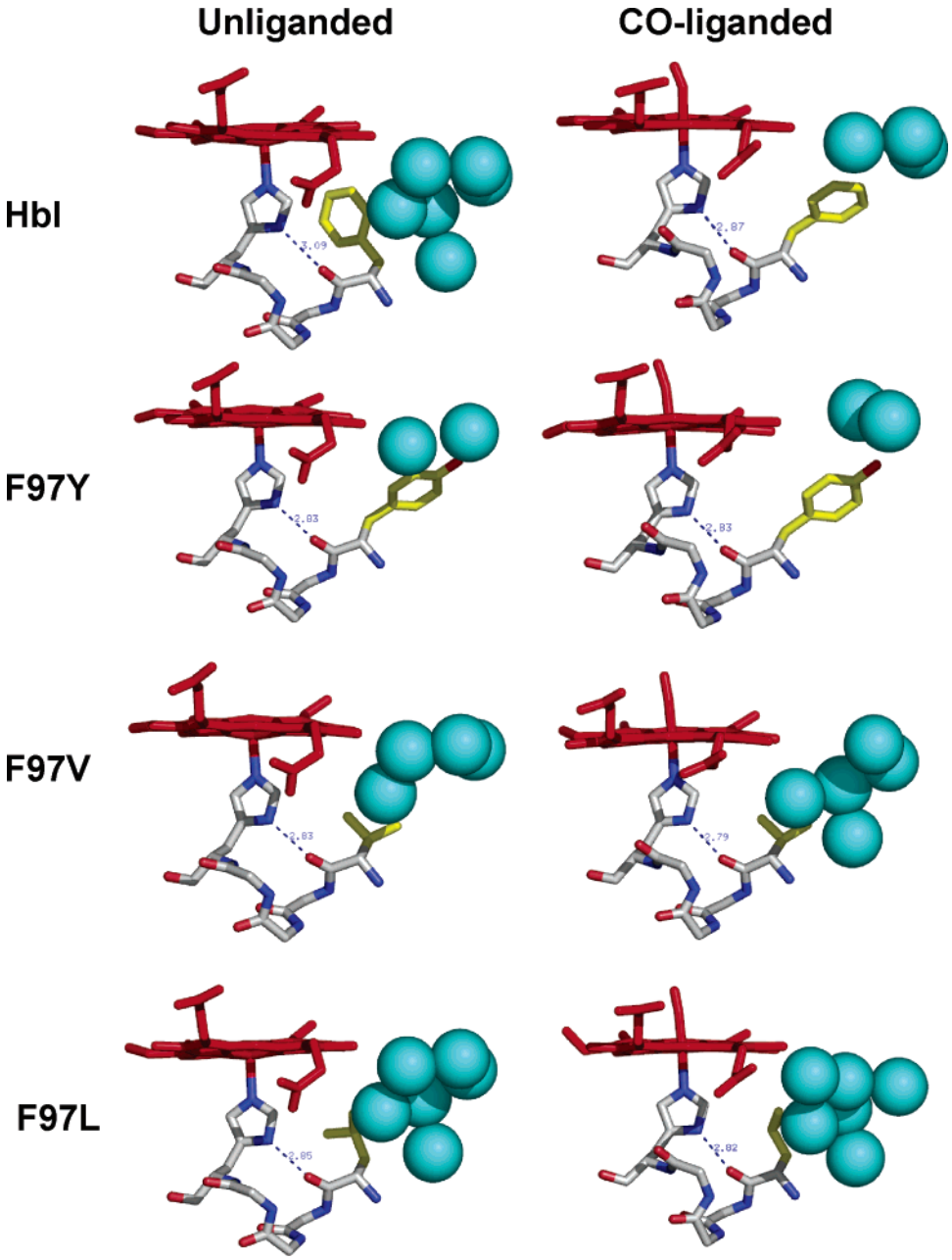


FIGURE 3: Structure of the region around the proximal heme pocket for wild-type HbI, F97Y, F97V, and F97L in both unliganded and CO-liganded forms. Heme and ligand atoms are colored red, and side chains of residue F4 are shown with yellow carbon atoms; proximal His (F8) and main chain atoms from F4 to F8 are depicted with conventional atom colors, and nearby interface water molecules shown as cyan van der Waals spheres. The potential hydrogen bond between the main chain F4 carbonyl oxygen and N$\delta$ of the proximal His is shown as a dashed line along with the N−O distance. Note the substantial conformational change by F4 Phe in wild-type HbI, along with the displacement of three neighboring ordered water molecules upon ligand binding. In F97Y, the Tyr side chain remains in the interface in both states, locking it into a conformation similar to the CO-liganded form. In F97V, the two $\gamma$-carbon atoms are oriented in a manner similar to that of the R and T state positions of HbI, whereas in F97L, ligand binding appears to be coupled with a rotation about the C$\beta$−C$\gamma$ bond. Despite displacement of three water molecules by F4 Phe, a central nucleus of five water molecules (three of which are shown here) is maintained in both states in HbI, but is not maintained intact in the three F4 mutants. Figures 3, 4, and 6 were produced with PYMOL (*34*).

and C rings (black in Figure 4), with an azimuthal angle of 30°, whereas in sperm whale myoglobin, the imidazole ring is quite "eclipsed", with an azimuthal angle of 1°. (A perfectly eclipsed orientation would have an azimuthal angle of 0°, whereas a perfectly staggered orientation would show an azimuthal angle of 45°.) An important functional impact of the azimuthal angle is that movement of the iron into the heme plane can be restricted by an eclipsed orientation, due to close contacts between imidazole atoms and pyrrole nitrogen atoms. This may contribute to the lower affinity of the T state in HbI, as the F8 imidazole takes on a more staggered orientation with the azimuthal angle dropping to 16°. Loosening the contact between F4 and F8 residues in the F4 mutants results in somewhat increased staggering in the T state, relative to that of the wild type, with the average value of the azimuthal angle of 19° in F97L, 17.5° in F97V, and 22° in F97Y.

*Ligand-Linked Heme Movement in F4 Mutants.* Ligand binding in wild-type HbI results in a movement of the heme groups deeper into each subunit and away from the subunit

Table 3: Packing Contacts within the Proximal Pocket

| | Phe 97 | Leu 97 | Val 97 | Tyr 97 |
|---|---|---|---|---|
| F4 (R state) | | | | |
| F4−CHB distance (Å) | 5.1 | 3.8 | 4.2 | 5.1 |
| F4−CMA distance (Å) | 3.7 | 4.1 | 5.2 | 3.8 |
| F4−His 101 distance (Å) | 4.8 | 3.6 | 3.7 | 3.9 |
| O97−Nδ101 distance (Å) | 2.8 | 2.9 | 2.8 | 2.8 |
| F8 (R state) | | | | |
| azimuthal angle (deg) | 29.9 | 31.0 | 29.7 | 33.6 |
| Fe−Nϵ distance (Å) | 2.07 | 2.07 | 2.06 | 2.09 |
| F4 (T state) | | | | |
| F4−CHB distance (Å) | 3.5 | 3.8 | 4.5 | 5.2 |
| F4−CMA distance (Å) | 4.4 | 4.0 | 5.2 | 3.9 |
| F4−His 101 distance (Å) | 3.3 | 3.4 | 3.9 | 5.0 |
| O97−Nδ101 distance (Å) | 3.1 | 2.9 | 2.9 | 2.9 |
| F8 (T state) | | | | |
| azimuthal angle (deg) | 15.7 | 19 | 17.4 | 22.2 |
| Fe−Nϵ distance (Å) | 2.08 | 2.08 | 2.03 | 2.04 |

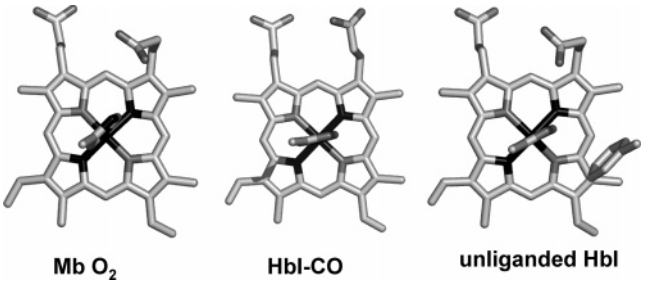


FIGURE 4: Orientation of the proximal His and heme in Mb and HbI. The heme and side chain of the proximal His are shown for the Mb−$O_2$ form (PDB entry 1MBO) (*35*) and HbI in the CO-liganded and unliganded structure, with the side chain for Phe F4 included in the unliganded HbI structure. Carbon atoms are colored light gray, nitrogen and oxygen atoms darker gray, and the heme iron and pyrrole nitrogen atoms from the A and C pyrrole rings black. Note the eclipsed orientation of the imidazole ring in the Mb−$O_2$ form compared with the nearly staggered orientation of the HbI−CO form, with the orientation of unliganded HbI between those two.

interface (*2*), a movement that has been suggested to be the trigger for the allosteric transition (*8*). A convenient measure of the heme position is the distance between the iron atoms in the dimer. In the CO-liganded structures of wild-type HbI and all three F97 mutants, the two iron atoms are 18.4 Å apart. The unliganded structures show more variation, with the two iron atoms 16.6 Å apart in wild-type HbI and F97L, 16.8 Å apart in F97V, and 17.2 Å apart in F97Y (Figure 5). Thus, the hemes do not move entirely to the normal T state position in F97Y, which can impact oxygen affinity, since the wild-type T state position of the heme iron results in steric interference with ligand binding (*8*). This heme position may contribute to the very high oxygen combination rate constants observed in F97Y (Figure 1 and Table 1).

*Interface Water Structure in F4 Mutants.* The very well ordered water molecules at the core of the dimeric interface of HbI undergo a large ligand-linked rearrangement and have been shown to be critical for stabilization of the HbI T state (*10*). Phe 97 plays a central role in the water rearrangement by directly displacing three water molecules when its side chain moves to the interface upon ligand binding (Figure 3). In the unliganded wild-type structure, there are 17 very well ordered water molecules (average *B*-factor of 19.6 Å$^2$, compared with an overall average protein side chain *B*-factor of 19.4 Å$^2$) at the central core of the dimer interface, while in the HbI−CO structure, there are 11 well ordered water molecules (average *B*-factor of 24.7 Å$^2$, with average side chain *B*-factors of 18.2 Å$^2$) as a result of displacement of three water molecules by each Phe 97. The Phe97 mutants have distinct effects on the interface water structure in the T and R states. In the unliganded structure of F97L, the core interface water molecules are in positions almost identical to those of the unliganded wild-type structure, although they are somewhat less well ordered with *B*-factors that average 29.5 Å$^2$ (average side chain *B*-factors of 23.4 Å$^2$) (*9*). In contrast, the core interface water molecules of the R state of F97L appear to be a hybrid of those of the T and R states of wild-type HbI, including 16 water molecules that are significantly less well ordered than the wild-type molecules (average *B*-factor of 34.5 Å$^2$, with average side chain *B*-factors of 19.8 Å$^2$).

The presence of two phenol rings in both the R state and T state interfaces in F97Y substantially alters the arrangement of core interface water molecules. In the CO-liganded structure, the hydroxyl group of each Tyr 97 side chain displaces an ordered water molecule such that only nine water molecules are present as core interface water molecules instead of the 11 that are found in the wild type. Loss of ligand causes many of the structural transitions observed in the wild type that impact the water structure, including the ligand-linked quaternary change, and subtle conformational changes of Arg 53, Lys 96, Asn 100, and Arg 104, but not those involving residue 97. This combination of changes results in the presence of only six water molecules being at the core of the T state interface of F97Y as compared to 17 water molecules present at the unliganded wild-type and F97L interfaces (Figure 6). One important caveat in the analysis of the interface water molecules is that the unliganded F97Y structure is at somewhat lower resolution (1.8 Å) than the CO-liganded form (1.5 Å). However, the observation of an extensive and well-ordered interface water structure in the crystal structure of unliganded F97L at 1.7 Å resolution (see above) argues that the observed reduction in the number of core interface water molecules in unliganded F97Y is significant. In addition, analysis of more than 20 unliganded HbI mutant structures, in which the mutation does not directly impact the interface, at limiting resolutions in the range of 1.8−2.1 Å invariably shows clear density for the full complement of interface water molecules first identified in studies of wild-type HbI at 1.6 Å resolution (J. E. Knapp and W. E. Royer, Jr., unpublished results). The reduction in the number of core interface water molecules in the unliganded structure of F97Y is due in part to the displacement of eight water molecules by the presence of a phenolic side chain in the unliganded interface, including two water molecules which occupy equivalent positions in both the R and T state structures of wild-type HbI. There are two additional water molecules that are displaced by the propionate group from the pyrrole A ring of the heme and one water molecule that appears to be absent due to a lack of hydrogen bonding with water molecules that were displaced as described above. The remaining water molecules that remain at the F97Y-unliganded interface are displaced from wild-type counterparts by 0.3−0.7 Å. Along with high *B*-factors, averaging 40.2 Å$^2$ for these water molecules, this suggests the unliganded interface of F97Y is much more fluid than the wild type.

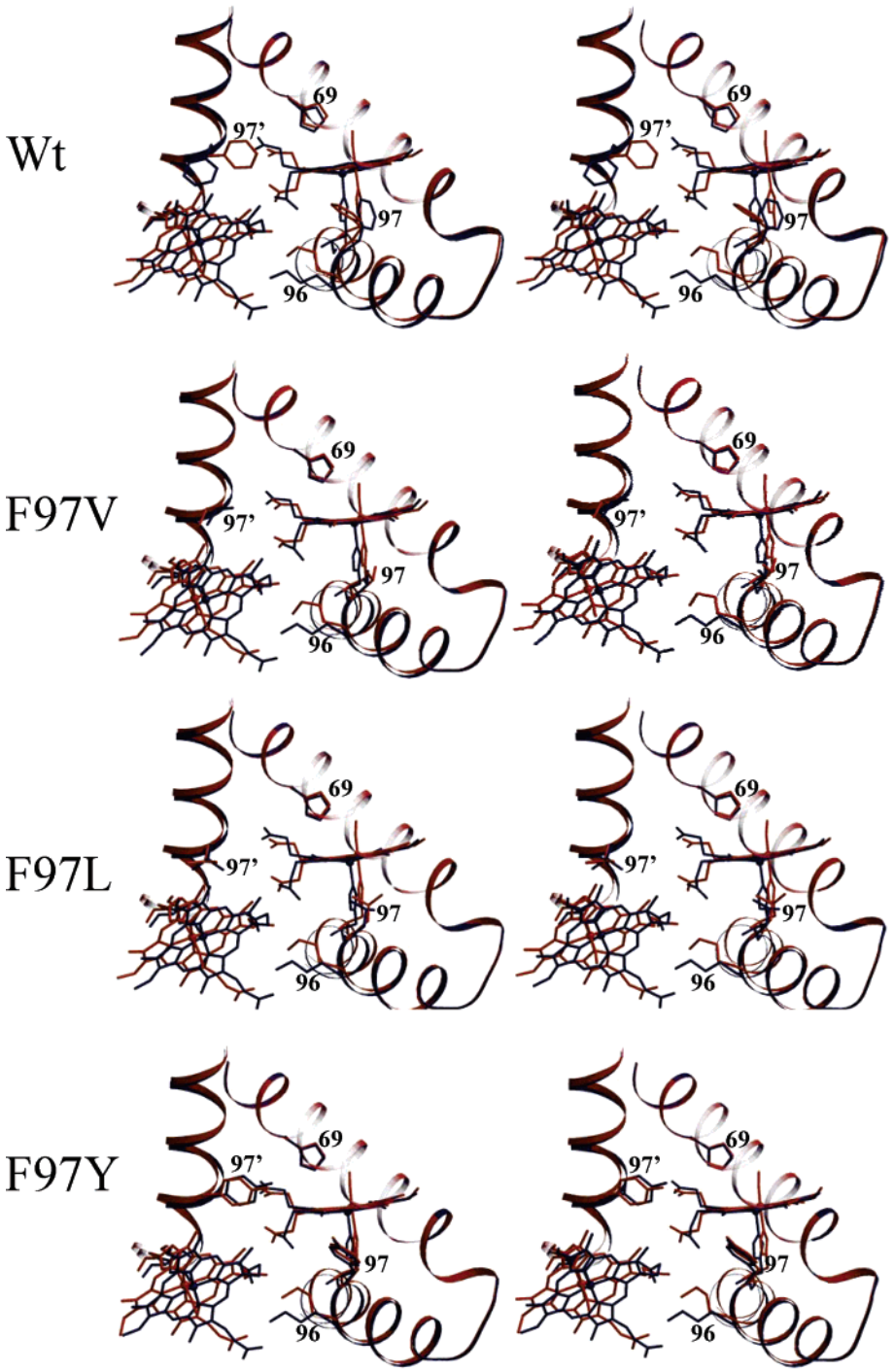


FIGURE 5: Stereoview of ligand-linked structural changes in F4 mutants. The E-helix from the A subunit of the unliganded state (blue) is superimposed upon its counterpart from the CO-liganded state (red) for the wild type, F97L, F97V, and F97Y. Side chains are included for residues 69 (distal His E7), 96 (F3), and 97 (F4) and the proximal histidine (F8). There is a large ligand-linked change of F4 in the wild type, but more limited changes in the conformations of the F97L, F97V, and F97Y mutants. It is apparent from this view that the bending of the F-helix as observed in the allosteric transition of the wild type is attenuated in each of the three F4 substitutions. Furthermore, the heme group positions of the two allosteric states are more similar in F97Y than in any of the other three transitions.

The water structure of the interface of the F97V−CO form is similar to that of the F97L−CO form, but differs from the CO-liganded form of the wild type. The F97V−CO interface includes 16 ordered water molecules, with eight of these having positions equivalent to their counterparts in the wild type. One additional water molecule has an altered position compared to its counterpart in the wild type. The F97V interface also includes six water molecules not present in the wild type but which are also present in the F97L−CO form. These six waters are located in the space that would normally be occupied by the Phe 97 side chain. There is only one water molecule missing in F97V, but present in both the wild type and F97L.

The water structure at the unliganded F97V interface includes only eight water molecules compared to 17 water molecules at the subunit interfaces of unliganded F97L and wild-type HbI. Three of the water molecules that are absent in F97V are displaced by the $\gamma$2-carbon atom of Val 97 as

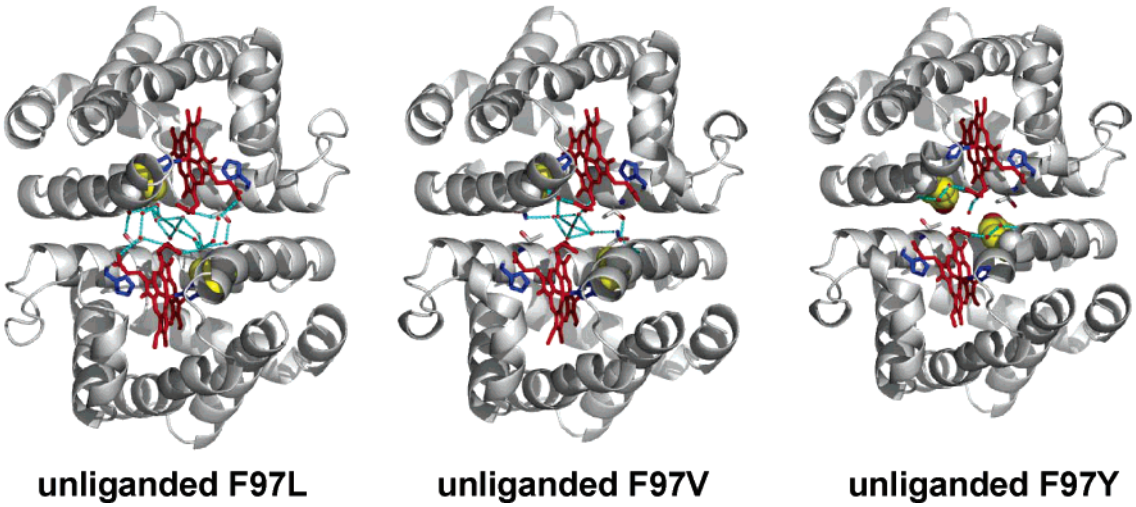


FIGURE 6: Core interface water hydrogen bonding network in unliganded F97L, F97V, and F97Y. The course of the polypeptide chain is depicted as a gray ribbon diagram, with hemes colored red, distal and proximal histidines blue, and side chains for residue Thr 72 and Asn 79 (F79V) gray and red, respectively; the interface water molecules are depicted as small red spheres, and residue F4 is depicted as yellow van der Waals surfaces (partially hidden). The hydrogen bonding network is colored cyan among interface water molecules and those side chains included in the figure. The interface water network for unliganded F97L is quite similar to that of the wild type and includes 17 well-ordered water molecules; that for unliganded F97V is less extensive, whereas the interface water network for unliganded F97Y is much less extensive and the most disordered.

each wild-type water would be 2.6−2.8 Å from this atom. (A fourth water molecule, symmetric to a displaced water molecule from one subunit, is located 3.1 Å from the $\gamma$2-carbon of Val 97 from the second subunit, and is present in the electron density maps.) The absence of the remaining four water molecules appears to arise from the loss of hydrogen bonding partners because of the three molecules displaced by the F97V mutation. The water molecules at the F97V interface are stable, exhibiting average *B*-factors of 27.3 Å$^2$. The *B*-factors are comparable to that within the F97L interface and are much lower than those for the F97Y interface water molecules.

## DISCUSSION

Phe 97 (F4) plays a central role in the allosteric mechanism of *Scapharca* HbI by undergoing a large ligand-dependent side chain rearrangement. The mutants presented here were designed to probe stereochemical parameters for control of ligand affinity in HbI by altering the residue at the F4 position. The mutations display dramatic functional alterations and include the highest-affinity mutant of HbI ever observed.

*Structural Basis for Ligand Affinity in F4 Mutants.* Substitution of F4 Phe with Val and Tyr results in 25−100-fold increases in oxygen affinity compared to that of wild-type HbI, and 3−12-fold increases in oxygen affinity compared to that of F97L. Furthermore, the reactivity of the heme iron, as measured by the CO combination rate constants, is increased in both of these mutations. On the basis of the structural analysis of the wild-type T state structure, two aspects of packing of Phe 97 against the heme and distal histidine have been proposed to contribute to the low-affinity conformation: steric restriction of the iron into the heme plane and lengthening of a key hydrogen bond between the proximal His N$\delta$ and the main chain carbonyl oxygen of residue F4 (*2*). All three F4 mutants exhibit very similar hydrogen bonding geometry between the F4 carbonyl oxygen and the proximal His. Therefore, differences in oxygen affinities among these mutations do not result from modulation of this hydrogen bond. Instead, differences in oxygen affinity appear to be more related to the side chain packing in the heme pocket, with decreases in mass packing against the proximal histidine and the B pyrrole ring of the heme correlated with higher affinity.

The variation in heme positions among the F4 mutants also may contribute to differences in oxygen affinity. The heme group in F97Y does not attain the full T state position. Heme groups in wild-type, F97L, and F97V T state structures are located in positions that are consistent with ligand binding being sterically hindered. Modeling bound CO onto the unliganded heme positions suggests a 2.1−2.2 Å distance between the oxygen atom of the ligand in the wild type, F97L, and F97V, whereas this distance increases to 2.4 Å for the unliganded F97Y structure. Reduction of the steric barrier to ligand binding may contribute to the higher oxygen combination rate constants observed for F97Y. The influence of the F4 residue in the proximal pocket on distal ligand interactions further supports the idea that the distal and proximal effects within HbI are coupled through the movement of the heme group, as suggested previously (*8*). Substitution of a Phe at position 114 prevents the heme group from moving to its R state position, while simultaneously locking Phe 97 in its T state position, demonstrating that these two allosterically important changes occur in a concerted manner (*8*).

Functionally important structural differences among F4 mutants also extend to the dimeric interface hydration. As shown in Figures 3 and 6, mutation at the F4 position results in alteration of the ordered interface water molecules, with the F97Y mutant exhibiting the most fluid water cluster. On the basis of molecular dynamics calculations (*27*) and mutagenesis (*8*), it has been suggested that the route for ligand migration may be quite different in HbI than in myoglobin. Such a difference could result from the involvement of the distal histidine in the dimeric interface, which would be likely to attenuate its flexibility and prevent

swinging into the solvent to permit ligand entry. The more fluid water arrangement in F97Y may release some of the restriction to the distal histidine movement and could open an additional channel for ligand migration past a swinging distal His. This effect, as well as the position of the heme groups noted above, may contribute to the very fast oxygen combination rates observed in F97Y (Figure 1 and Table 1).

*Organization of Interface Water Structure.* Mutation of the F4 residue provides a useful probe of the interface water structure, which has been shown to be functionally important in HbI (*10*). In the unliganded HbI structure, a very well ordered cluster of 17 water molecules contributes to T state stability. Movement of each Phe 97 into the interface upon ligand binding displaces three water molecules, which is part of an overall rearrangement into 11 core interface water molecules. Despite such a dramatic rearrangement, five water molecules are unaltered by the T to R transition and form a nucleus onto which the alternate water structures are assembled. Introduction of a Tyr into the interface in the F97Y structure substantially alters the interface water arrangement, including disrupting the central nucleus. In the R state, nine well-ordered water molecules can still be accommodated, but differences in the unliganded structure are more drastic with only six substantially less well ordered water molecules present. Apparently, the core interface water structure of the T state is incompatible with the presence of a Tyr side chain in the interface. This provides an indication of the exquisite organization of the HbI dimeric interface to be able to maintain well-ordered, albeit rearranged, water networks in the presence and absence of a phenyl side chain in the interface.

*Control of Ligand-Linked Heme Group Movement.* Although movement of the heme group appears to be the trigger that initiates allosteric transitions within *Scapharca* Hb, aspects of the driving forces for this movement remain elusive. The bound ligand itself has been suggested to contribute to the movement of the heme from its T state to R state, due to its contacts with the distal His (*8*), an idea that is consistent with attenuation of this heme movement in mutants of the distal His (J. E. Knapp, W. E. Royer, Jr., Q. H. Gibson, manuscript in preparation). It is, however, unclear what drives an unliganded heme from its R to T state position. F97Y is the first HbI mutant in which the unliganded heme does not attain a normal T state position, rather it undergoes ~70% of the wild-type R to T state transition. This implies that Tyr 97, which remains in the interface in both states, interferes with the T state positioning of the heme group. There are three plausible structural changes that could contribute to the altered unliganded heme position: (1) shifts in the F-helix, (2) removal of packing contacts in the unliganded F97Y heme pocket, and (3) alterations in the subunit interface. Comparison of the wild type and F4 mutants show that all three mutants shift the F-helix by ~0.2 Å in each subunit, suggesting that if this were the cause of the attenuated heme movement, all F4 mutants, not just F97Y, should show attenuated heme movement. Likewise, the packing contacts observed in unliganded HbI are missing in both F97V and F97Y. Thus, it appears unlikely that stereochemical alterations in the heme pocket of each subunit are responsible for the anomalous heme movement of F97Y. On the other hand, F97Y is unique in the nature of its T state interface, with the least organized water cluster, as discussed above. Ordered water molecules that are observed to form hydrogen bonds with the heme propionates in other unliganded structures are not found in the unliganded F97Y interface. This raises the possibility that the ordered water molecules in the dimeric interface of the T state HbI structure may play a critical role in facilitating the heme group movement to its normal T state position.

*F97Y as a Mimic for the R State.* Comparisons of mutations that approach an allosteric end point offer the potential to contribute to our understanding of the functional ramifications of the allosteric transition in HbI. F97Y is the highest-affinity HbI mutant constructed to date and possesses many of the structural attributes of the R state, even in the absence of ligand. A useful comparison can be made with another high-affinity mutant, T72V, in which the interface water structure of the T state is destabilized. T72V undergoes the complete HbI allosteric transition (*28*) and exhibits high levels of cooperativity for oxygen binding, results that can be fully interpreted in the context of the MWC model in which the allosteric constant $L$ is drastically reduced due to the destabilization of the T state (*10*). On the basis of the analysis of oxygen/CO replacement data similar to that described here for the Phe 97 mutants, the rate constant for binding the second oxygen ($k_2'$) is estimated to be 50 $\mu M^{-1}$ $s^{-1}$, whereas the oxygen dissociation constant for the doubly liganded form ($k_2$) is estimated to be 3 $s^{-1}$. The similarity of these values with those for F97Y (Table 1) supports the notion that F97Y is locked in the R state. These results strongly support an earlier suggestion, based on the MWC model (*15*), of an approximately 300-fold difference between R and T state affinities (*10*). This suggests that F97Y can be considered a reasonable mimic for the R state of HbI, and its 100-fold increase in oxygen affinity relative to that of the wild type illustrates the very strong functional impact of the R to T transition in HbI that is achieved despite relying on relatively localized tertiary transitions.

*Comparison with Myoglobin.* The F4 position of sperm whale myoglobin, occupied by a leucine in the wild type, has also been investigated by mutagenesis (Figure 7). Mutation of Leu F4 to Gly increases oxygen affinity by 1.2-fold; on the other hand, the introduction of Phe decreases the oxygen affinity by a factor of 1.7, and Trp decreases oxygen affinity by 4-fold. Thus, mutations at this position in myoglobin ranging from very small (Gly) to very large (Trp) result in a less than 5-fold difference in oxygen affinity. In contrast, mutations at the F4 position in HbI result in a 100-fold change in oxygen affinity. Why is HbI so much more sensitive to the size of the residue at position F4 than sperm whale myoglobin? A likely key contributor is the orientation of the proximal histidine and the heme group. As shown in Figure 4, the proximal histidine for myoglobin is in an eclipsed orientation relative to the heme pyrrole nitrogen atoms of the A and C rings (with an azimuthal angle of 1°), whereas in the CO derivative of HbI, the proximal histidine takes a more staggered orientation (azimuthal angle of 29−31°). In an eclipsed orientation, movement of the heme iron into the heme plane is somewhat restricted by tight contacts between the histidine imidazole ring atoms and the heme pyrrole nitrogen atoms, an effect that becomes more pronounced if the proximal histidine is tilted relative to the

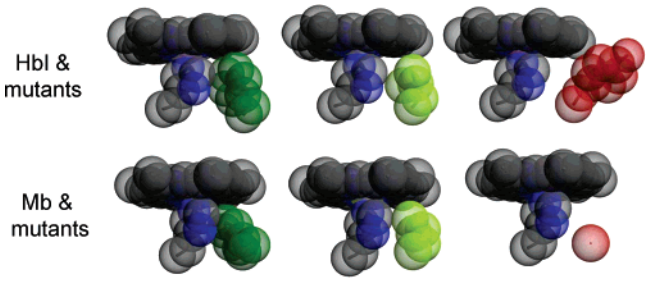


FIGURE 7: Proximal pockets of wild-type HbI (top) and sperm whale myoglobin (Mb). Structures of wild-type HbI (left), F97L (middle), and F97Y (right) are shown with the van der Waals radii drawn to scale. Mb structures with equivalent side chains based on packing contacts are shown below. This includes wild-type Mb (middle) along with its L89F (left) and L89G (right) mutants. F97L (light green) packs into the proximal pocket in a manner similar to that of sperm whale Mb, whereas the disposition of the Phe at position F4 (dark green) in both these globins is quite different. Nevertheless, both aromatic rings pack tightly against the porphyrin ring, with comparable packing contacts. Both F97Y in HbI and L89G in Mb (with F4 in red) have no direct contact with the porphyrin ring. Despite the structural similarities between equivalent substitutions, the oxygen affinity differences between these mutations vary by 100-fold in HbI and only 5-fold in Mb.

heme normal. This effect was elegantly shown in Barrick's replacement of the proximal histidine by free imidazole using his H93G mutation, in which a bound imidazole, unrestrained by the polypeptide, attains a staggered orientation and moves closer to the heme than the proximal histidine (*29*). Restricted iron motion will lower the heme reactivity, due to the strain induced in bringing the heme iron atom into a position to bind six ligands in an octahedral coordination. In contrast, the more staggered orientation of the proximal histidine in HbI potentially allows higher intrinsic oxygen affinity, but also permits other stereochemical strategies that limit iron motion to have a large impact on oxygen affinity. Alteration of the packing of the F4 side chain in the heme pocket has a profound effect on oxygen affinity, as illustrated by the mutations presented here. This provides *Scapharca* HbI with a mechanism for strongly modulating oxygen affinity based on alternate proximal pocket structures.

These comparisons highlight the strategy used by *Scapharca* HbI that is strikingly different from that employed by mammalian hemoglobins, despite sharing modulation of proximal stereochemistry as an allosteric mechanism. A relatively staggered arrangement of the proximal histidine in mammalian hemoglobins, although not as staggered as observed in sperm whale myoglobin, renders oxygen affinity particularly sensitive to the tilt of the histidine relative to the heme plane (*30*). A significant tilt, coupled with an eclipsed orientation, restricts movement of the heme iron into the heme plane due to tight contacts between the imidazole and pyrrole nitrogen atoms. In this way, oxygen affinity can be strongly affected by the position of the F-helix, which acts as a link between the tilt of the proximal histidine and key intersubunit contacts. In contrast, F4 Phe in *Scapharca* hemoglobin can modulate oxygen affinity by inhibiting movement of the iron into the heme when packed in the proximal pocket with a more eclipsed proximal His orientation and releasing this constraint by being expelled from the pocket leaving a more staggered orientation of the proximal His.

## ACKNOWLEDGMENT

We thank Betha Komali and Tina Nguyen for technical assistance.

## REFERENCES

1. Chiancone, E., Vecchini, P., Verzili, D., Ascoli, F., and Antonini, E. (1981) Dimeric and tetrameric hemoglobins from the mollusc *Scapharca inaequivalvis*. Structural and functional properties, *J. Mol. Biol. 152*, 577−92.
2. Royer, W. E., Jr. (1994) High-resolution crystallographic analysis of a co-operative dimeric hemoglobin, *J. Mol. Biol. 235*, 657−81.
3. Perutz, M. F. (1979) Regulation of oxygen affinity of hemoglobin: Influence of structure of the globin on the heme iron, *Annu. Rev. Biochem. 48*, 327−86.
4. Mitchell, D. T., Kitto, G. B., and Hackert, M. L. (1995) Structural analysis of monomeric hemichrome and dimeric cyanomet hemoglobins from *Caudina arenicola*, *J. Mol. Biol. 251*, 421−31.
5. Royer, W. E., Jr., Heard, K. S., Harrington, D. J., and Chiancone, E. (1995) The 2.0 Å crystal structure of *Scapharca* tetrameric hemoglobin: Cooperative dimers within an allosteric tetramer, *J. Mol. Biol. 253*, 168−86.
6. Royer, W. E., Jr., Strand, K., van Heel, M., and Hendrickson, W. A. (2000) Structural hierarchy in erythrocruorin, the giant respiratory assemblage of annelids, *Proc. Natl. Acad. Sci. U.S.A. 97*, 7107−11.
7. Flores, J. F., Fisher, C. R., Carney, S. L., Green, B. N., Freytag, J. K., Schaeffer, S. W., and Royer, W. E., Jr. (2005) Sulfide binding is mediated by zinc ions discovered in the crystal structure of a hydrothermal vent tubeworm hemoglobin, *Proc. Natl. Acad. Sci. U.S.A. 102*, 2713−8.
8. Knapp, J. E., Gibson, Q. H., Cushing, L., and Royer, W. E., Jr. (2001) Restricting the ligand-linked heme movement in *Scapharca* dimeric hemoglobin reveals tight coupling between distal and proximal contributions to cooperativity, *Biochemistry 40*, 14795−805.
9. Pardanani, A., Gibson, Q. H., Colotti, G., and Royer, W. E., Jr. (1997) Mutation of residue Phe97 to Leu disrupts the central allosteric pathway in *Scapharca* dimeric hemoglobin, *J. Biol. Chem. 272*, 13171−9.
10. Royer, W. E., Jr., Pardanani, A., Gibson, Q. H., Peterson, E. S., and Friedman, J. M. (1996) Ordered water molecules as key allosteric mediators in a cooperative dimeric hemoglobin, *Proc. Natl. Acad. Sci. U.S.A. 93*, 14526−31.
11. Knapp, J. E., and Royer, W. E., Jr. (2003) Ligand-linked structural transitions in crystals of a cooperative dimeric hemoglobin, *Biochemistry 42*, 4640−7.
12. Summerford, C. M., Pardanani, A., Betts, A. H., Poteete, A. R., Colotti, G., and Royer, W. E., Jr. (1995) Bacterial expression of *Scapharca* dimeric hemoglobin: A simple model system for investigating protein cooperatively, *Protein Eng. 8*, 593−9.
13. Hayashi, A., Suzuki, T., and Shin, M. (1973) An enzymic reduction system for metmyoglobin and methemoglobin, and its application to functional studies of oxygen carriers, *Biochim. Biophys. Acta 310*, 309−16.
14. Scott, E. E., and Gibson, Q. H. (1997) Ligand migration in sperm whale myoglobin, *Biochemistry 36*, 11909−17.
15. Monod, J., Wyman, J., and Changeux, J. P. (1965) On the Nature of Allosteric Transitions: A Plausible Model, *J. Mol. Biol. 12*, 88−118.
16. Otwinowski, Z., and Minor, W. (1997) Processing of X-ray diffraction data collected in oscillation mode, *Methods Enzymol. 276*, 307−26.
17. Collaborative Computational Project Number 4 (1994) The CCP4 Suite: Programs for Protein Crystallography, *Acta Crystallogr. D50*, 760−3.
18. Brunger, A. T. (1992) Free *R* value: A novel statistical quantity for assessing the accuracy of crystal structures, *Nature 355*, 472−5.
19. Brunger, A. T. (1992) *X-PLOR*, version 3.1, Yale University Press, New Haven, CT.
20. Brunger, A. T., Adams, P. D., Clore, G. M., DeLano, W. L., Gros, P., Grosse-Kunstleve, R. W., Jiang, J. S., Kuszewski, J., Nilges, M., Pannu, N. S., Read, R. J., Rice, L. M., Simonson, T., and

Warren, G. L. (1998) Crystallography & NMR system: A new software suite for macromolecular structure determination, *Acta Crystallogr. D54* (Part 5), 905−21.
21. Jones, T. A., Zou, J. Y., Cowan, S. W., and Kjeldgaard, M. (1991) Improved methods for building protein models in electron density maps and the location of errors in these models, *Acta Crystallogr. A47* (Part 2), 110−9.
22. Berman, H. M., Westbrook, J., Feng, Z., Gilliland, G., Bhat, T. N., Weissig, H., Shindyalov, I. N., and Bourne, P. E. (2000) The Protein Data Bank, *Nucleic Acids Res. 28*, 235−42.
23. Kleywegt, G. J. (1996) Use of non-crystallographic symmetry in protein structure refinement, *Acta Crystallogr. D52*, 842−57.
24. Vojtechovsky, J., Chu, K., Berendzen, J., Sweet, R. M., and Schlichting, I. (1999) Crystal structures of myoglobin-ligand complexes at near-atomic resolution, *Biophys. J. 77*, 2153−74.
25. Liong, E. C., Dou, Y., Scott, E. E., Olson, J. S., and Phillips, G. N., Jr. (2001) Waterproofing the heme pocket. Role of proximal amino acid side chains in preventing hemin loss from myoglobin, *J. Biol. Chem. 276*, 9093−100.
26. Valentine, J. S., Sheridan, R. P., Allen, L. C., and Kahn, P. C. (1979) Coupling between oxidation state and hydrogen bond conformation in heme proteins, *Proc. Natl. Acad. Sci. U.S.A. 76*, 1009−13.
27. Chiancone, E., Elber, R., Royer, W. E., Jr., Regan, R., and Gibson, Q. H. (1993) Ligand binding and conformation change in the dimeric hemoglobin of the clam *Scapharca inaequivalvis*, *J. Biol. Chem. 268*, 5711−8.
28. Pardanani, A., Gambacurta, A., Ascoli, F., and Royer, W. E., Jr. (1998) Mutational destabilization of the critical interface water cluster in *Scapharca* dimeric hemoglobin: Structural basis for altered allosteric activity, *J. Mol. Biol. 284*, 729−39.
29. Barrick, D. (1994) Replacement of the proximal ligand of sperm whale myoglobin with free imidazole in the mutant His-93 → Gly, *Biochemistry 33*, 6546−54.
30. Perutz, M. F., Fermi, G., Luisi, B., Shaanan, B., and Liddington, R. C. (1987) Stereochemistry of cooperative mechanisms in hemoglobin, *Cold Spring Harbor Symp. Quant. Biol. 52*, 555−65.
31. Adair, G. S. (1925) The hemoglobin system: VI. The oxygen dissociation curve of hemoglobin, *J. Biol. Chem. 63*, 529−45.
32. Esnouf, R. M. (1999) Further additions to MolScript version 1.4, including reading and contouring of electron-density maps, *Acta Crystallogr. D55* (Part 4), 938−40.
33. Merritt, E. A., and Bacon, D. J. (1997) Raster3D: Photorealistic molecular graphics, *Methods Enzymol. 277*, 505−24.
34. DeLano, W. L. (2002) The Pymol Molecular Graphics System, DeLano Scientific, South San Francisco, CA.
35. Phillips, S. E. (1980) Structure and refinement of oxymyoglobin at 1.6 Å resolution, *J. Mol. Biol. 142*, 531−54.

BI051052+